REACTIVE HYPERSONIC FLOWS COMPUTED WITH DETAILED CHEMICAL KINETICS MODELS

Marie-Claude Druguet, Arnaud Bultel, Vincent Morel, Julien Annaloro

53rd 3AF International Conference on Applied Aerodynamics
26 – 28 March 2018, Salon de Provence, France

FP58-AERO2018-druguet

REACTIVE HYPERSONIC FLOWS COMPUTED WITH DETAILED CHEMICAL KINETICS MODELS

Marie-Claude Druguet [(1)], Arnaud Bultel[(2)], Vincent Morel[(3)] and Julien Annaloro[(4)]
[(1)]*Aix-Marseille Univ., CNRS UMR 7343, IUSTI, 5 rue Enrico Fermi, Marseille, 13453, France*
Email: marie-claude.druguet@univ-amu.fr
[(2)]*Normandie University, CNRS UMR 6614, CORIA, Site du Madrillet, St Etienne du R., 76801, France*
Email: arnaud.bultel@coria.fr
[(3)]*Poitiers University, CNRS UPR 3346, PPRIME, ISAE-ENSMA, Futuroscope, 86962, France*
Email: morel@coria.fr
[(4)]*CNES, DCT/TV/PR, BPI 1717, 18 Avenue Edouard Belin, Toulouse, 31401, France*
Email: julien.annaloro@cnes.fr

ABSTRACT

The present work shows the ability of Navier-Stokes codes to handle detailed chemical kinetics models to compute the reactive and vibrational non-equilibrium gases in shock layers and the recent development done in our laboratories towards this goal. The detailed model used in the present study is a simplified version of a collisional-radiative model for N_2 that has been implemented step-by-step in a Navier-Stokes code in order to show the effect of each group of chemical and vibrational processes. The processes taken into account are the vibration—vibration exchanges and the vibration—translation exchanges through molecular or atomic impact, leading to dissociation or not. The question of how the vibrational levels reach the Boltzmann distribution is also assessed. Comparisons of results obtained with global and detailed chemical kinetics models are presented.

1. INTRODUCTION

If simulating non-equilibrium gas flows in shock layers has been widely done so far with global models for the chemical reactions and the vibrational non-equilibrium relaxation, it is new to compute such flow fields with detailed chemical kinetics models. This is now possible as the CPU and memory resources of the computers allow running CFD codes with detailed models. State-specific vibrational models are efficient to model both the chemical reactions and the vibrational non-equilibrium at once, without making strong assumptions (like Boltzmann distribution) as it is the case with multi-temperature models for vibrational non-equilibrium modeling.

A major step has been done recently by IUSTI and CORIA in simulating the reactions between chemical species on their vibrational excited states (called pseudo species) and the evolution of these pseudo species in the shock layer surrounding a sphere flying into a nitrogen gas at a speed of 10.6 km/s, modeled by means of a simplified version of CoRaM-N_2, a collisional-radiative (CR) model developed by CORIA [1]. This simplified model was recently implemented in the CFD code PINENS developed at IUSTI [2,3], in which the shock resolution is done with a shock-capturing method, an approximate Riemann solver in a finite-volume discretization of the Navier-Stokes equations.

2. STATE-TO-STATE MODELING

2.1 Chemical Species and Vibrational Energy States

The vibrationally specific model subject of the present work is a simplified version of the collisional-radiative model CoRaM-N_2. It takes into account heavy, neutral particles and considers each of the 68 vibrational states of N_2 ($v = 0 \rightarrow 67$) on the ground electronic state as pointed out by Armenise et al. [4], as well as N ground electronic state (Tab. 1). Those states represent the 69 pseudo species whose population density evolutions are to be computed with a Navier-Stokes code.

Table 1. Species and vibrational states considered in the present vibrational-state specific model.

Species	States
$N_2(v)$	v = 1 → vmax = 67 for ground electronic state
N	ground electronic state

2.2 Collisional Elementary Processes

According to the CR model CoRaM-N_2 that is used as the basis to derive the present vibrational-state specific model, the vibrational excitation of molecules N_2 takes place through vibration—vibration processes under molecular impact (VV-m, 4489 processes), through vibration—translation processes under molecular impact (VT-m, 67 processes), or through vibration—translation processes under atomic impact (VT-a, 2125 processes). The data used for the rate coefficients for these processes were calculated by Esposito et al. [4] and Armenise et al. [5]. Once vibrationnally excited, the molecules N_2 may dissociate during collisions. For the dissociation of N_2 through vibration—vibration processes under molecular impact (VV-m-D, 67 processes), through vibration—translation processes under molecular impact (VT-m-D, 1 process), or through vibration—translation process under atomic impact (VT-a-D, 68 processes), the data of Esposito et al. [4] and those of Armenise et al. [5] are also used. The total number of processes is 6817 forward reactions that are summarized in Tab. 2. The backward collisional elementary processes are calculated from the forward rate coefficient and the corresponding equilibrium constant using the detailed balance principle. Thus, the set represents a total of about 13,600 forward and backward elementary processes between 69 pseudo species.

Table 2: Elementary processes for the present vibrational-state specific model.

Elementary processes	Process number
Vibration-vibration under molecular impact (VV-m)	4489
Vibration-translation under molecular impact (VT-m)	67
Vibration-translation under molecular impact leading to dissociation (VT-m-D)	1
Vibration-vibration under molecular impact leading to dissociation (VV-m-D)	67
Vibration-translation under atomic impact (VT-a)	2125
Vibration-translation under atomic impact leading to dissociation (VT-a-D)	68

3. GLOBAL MODELING

When modeling a chemically and vibrationally non-equilibrium nitrogen flow with global models, the chemical species and vibrational energies listed in Tab. 3 are considered.

Table 3. Species and vibrational energy considered in the global model.

Species	Vibrational energy
N_2	e^V_{N2}
N	-

This is well known, but recalled here to compare the completeness of a detailed model as presented in Section 2 to the simplicity of a global model.

3.1 Chemical Kinetics

The global chemical kinetics model for a mixture composed of the 2 species N_2 and N is a set of 2 dissociation-recombination reactions, as shown in Tab. 4. This is what is usually used in CFD codes for hypersonic entry flows in a nitrogen atmosphere.

Table 4. Global chemical kinetics model.

Chemical processes
$N_2 + N_2 \leftrightarrow N + N + N_2$
$N_2 + N \leftrightarrow N + N + N$

3.2 Vibrational Relaxation

Multi-temperature models are usually used in CFD codes to model the vibrational relaxation of molecular species. These models are based on solving one conservation equation of vibrational energy for each vibrating molecule, in the same way as mass conservation equations are solved for every chemical species. The source term for the vibrational energy conservation equations is derived according to the Landau-Teller model [6], in which the characteristic time of vibrational relaxation is computed according to Millikan and White [7].

4. RESULTS AND ANALYSIS

Results obtained with Navier-Stokes simulations performed with the PINENS code are the spatial evolution of N_2 and N concentrations throughout the axi-symmetric shock layer past a 1-meter radius sphere flying at 10.6 km/s, for the 68 vibrational states of N_2 and the fundamental electronic state of N.

4.1 VV-m: 4489 Processes

The first step in analyzing the effect of each group of processes — summarized in Tab. 2 — on the flow field (temperature, species densities, ...) consists in considering the processes for the vibration—vibration exchanges by molecular impact (VV-m). Surprisingly, introducing the reactions corresponding to these processes does not produce any visible effect on the temperature nor on the pseudo species profiles in the shock layer. The shock position, the temperature, and the total density evolutions throughout the shock layer are the same when VV-m processes are taken into account as when no chemical processes are taken into account. Therefore, these processes are omitted in the following computations.

4.2 VT-m: 67 Processes

The second step in analyzing the effect of a group of processes on the flow field and on the vibrational-level population densities consists in taking into account the vibration—translation exchanges by molecular impact (VT-m). Interestingly, the temperature contours around the sphere (Fig. 1) or the temperature profile along the stagnation line (Fig. 2), are very similar to the results that are obtained when no chemical reactions are taken into account in the gas flow: the temperature is maximum in the entire shock layer, with a maximum reached near the stagnation area of the flow, right before the boundary layer. This means that the VT-m processes do not take much thermal energy from the gas. The evolutions of the mass fractions of each vibrational level of N_2 (from v = 0 to 67) along the stagnation line throughout the shock layer, including the boundary layer, are also shown in Fig. 2. The fundamental vibrational level of N_2 (v=0) is depopulated across the shock wave to the profit of the excited states v=1 to 67. As this is expected, the lowest levels are the most populated levels. The behavior of the first 10 vibrational levels right behind the shock wave is interesting: their population increases in the shock front, then decreases only 1 mm behind the shock front, to the profit of the excitation of higher vibrational states. The vibrational excitation process takes place as a cascade from the lower levels to the upper levels.

The contours of the vibrational levels v=0 and v=10 of N_2 are displayed in Figs. 3 and 4, as two samples of the vibrational level concentrations throughout the shock layer surrounding the sphere flying at hypersonic speed. It is clear that level v=10 is much less populated than the level v=0, and levels above v=10 are even less populated.

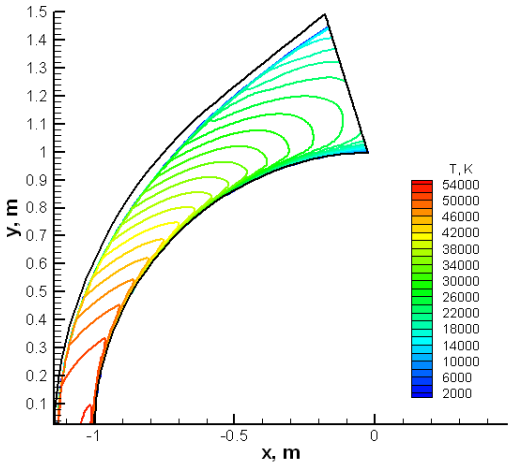

Figure 1. Temperature contours.
67 processes (VT-m) are included in the computations.
Effect of the VT excitation by molecular impact.

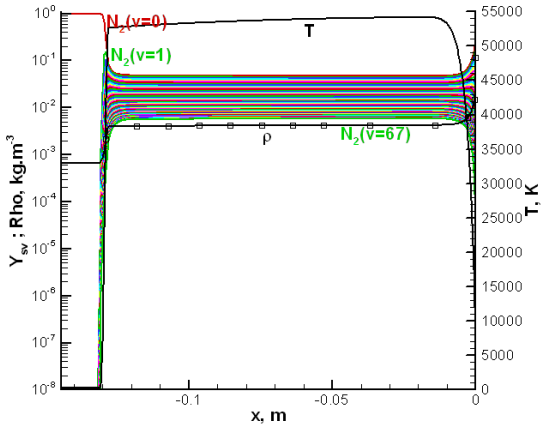

Figure 2. Temperature and mass fractions of
N_2 (v=0,67) and N along the stagnation line.
67 processes (VT-m) are included in the computations.
Effect of the VT excitation by molecular impact.

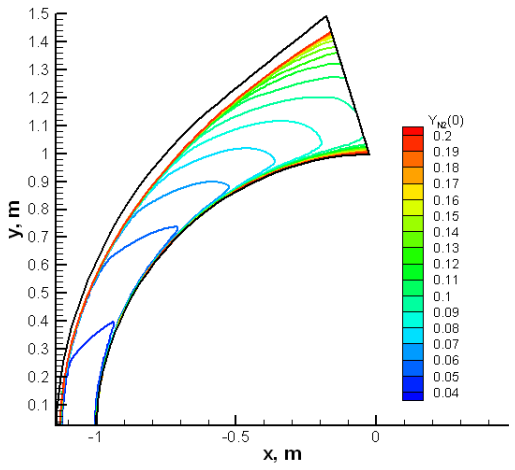

Figure 3. N_2(v=0) population density contours.
67 processes (VT-m) are included in the computations.
Effect of the VT excitation by molecular impact.

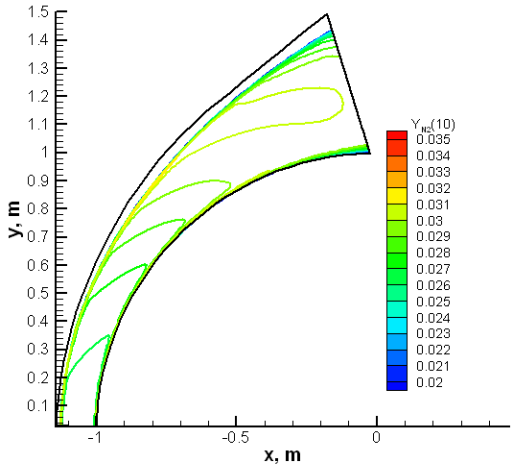

Figure 4. N_2(v=10) population density contours.
67 processes (VT-m) are included in the computations.
Effect of the VT excitation by molecular impact.

4.3 VT-m + VT-m-D: 68 Processes

The addition of the sole vibration—translation process by molecular impact leading to the dissociation (VT-m-D) leads to reduce the shock layer width from approximately 13 cm down to 10.5 cm (Fig. 5, compared to Fig. 2). The introduction of this single process into the computations also changes the temperature profile across the shock layer: the temperature is no longer maximum at 54,000 K throughout the shock layer but peaks at 50,000 K right behind the shock front then decreases. This temperature profile is similar to the temperature profiles usually observed when chemical reactions are taken into account through global models, and is typical of shock layers where dissociation processes take place. Regarding the species profiles within the shock layer, the atomic nitrogen N is now the major species present in the shock layer. All the vibrational levels of N_2 are less populated than in Fig. 2, especially the highest levels - because of the dissociation of N_2 from the highest vibrational levels - to the profit of the atomic species. This means that the VT-exchange by molecular impact leading to dissociation (process VT-m-D) is a very efficient process among the many reactions of the vibrationally specific model summarized in Tab. 2 and implemented in the CFD code. This reaction of dissociation of N_2(v) also absorbs a large amount of thermal energy : the temperature that was approximately equal to 54,000 K in the shock layer 1 cm from the stagnation point (see Fig. 2) is now equal to 23,000 K at the same location (Fig. 5).

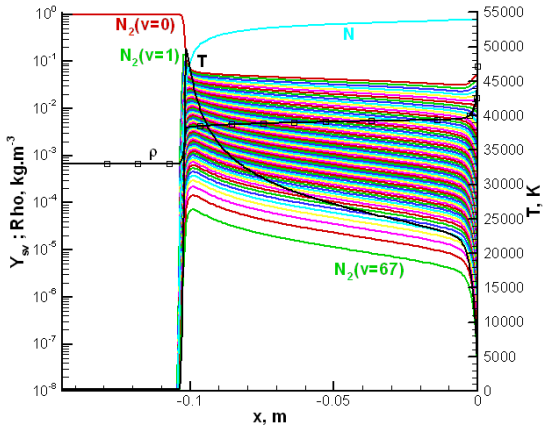

Figure 5. Temperature and mass fractions of
N_2 (v=0,67) and N along the stagnation line.
68 processes (VT-m + VT-m-D) are included in the computations.
Effect of the dissociation process through VT exchanges by molecular impact.

4.4 VT-m + VT-m-D + VV-m-D: 135 Processes

When the processes of vibration—vibration exchanges through molecular impact leading to dissociation (VV-m-D) are added to the processes VT-m + VT-m-D in the simulations, the results are the same as when only the processes VT-m + VT-m-D are taken into account. This shows that the VV processes (leading to dissociation or not, as discussed in Section 3.1) are not efficient in the present test-case.

4.5 VT-m + VT-m-D + VV-m-D + VT-a: 2260 Processes

The introduction of the 2125 processes of vibration—translation exchanges by atomic impact (VT-a) has a large effect on the flow field (Fig. 6 compared to Fig. 5, and Figs. 7-9, compared to Figs. 1, 3, 4). The reactions VT-a, like the process VT-m-D, lead to decreasing the shock layer width (from 10.5 cm to 8.5 cm approximately) and the temperature in the shock front peaks from 50,000 K (Fig. 5) down to 43,000 K (Fig. 6). Regarding the population densities in the shock layer, it is clear that the highest vibrational levels of N_2 are even more depopulated to the profit of atomic nitrogen production than they were before. The curve of N population density (Fig. 6) shows that there is more N production in the shock layer when processes VT-a are considered, although there is no additional reaction of dissociation (only the VT-m-D reaction that was introduced before).

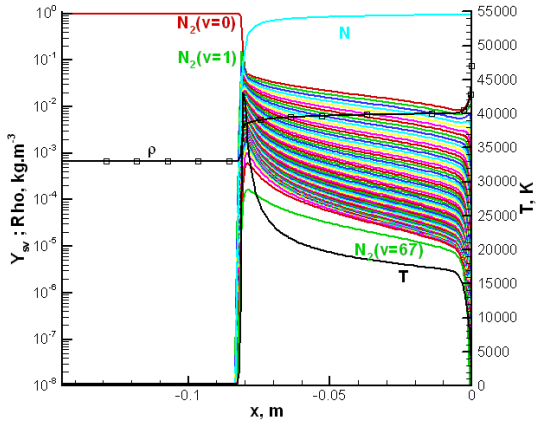

Figure 6. Temperature and mass fractions of N_2 (v=0,67) and N along the stagnation line.
2260 processes (VT-m + VT-m-D + VV-m-D + VT-a) are included in the computations.
Effect of the VT excitation by atomic impact :
2125 processes VT-a are included in the computations in addition to the 135 other processes included before.

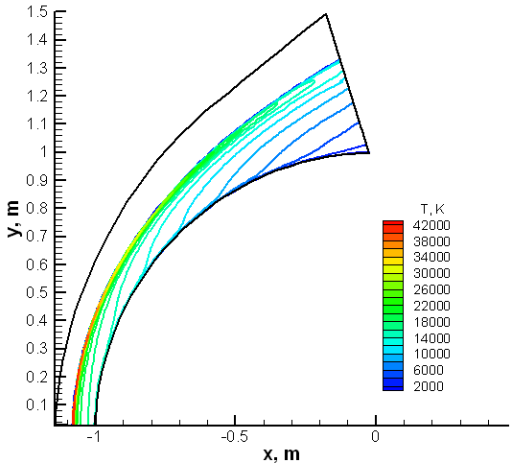

Figure 7. Temperature contours.
2260 processes (VT-m + VT-m-D + VV-m-D + VT-a) are included in the computations.
Effect of the VT excitation by atomic impact :
2125 processes VT-a are included in the computations in addition to the 135 other processes included before.

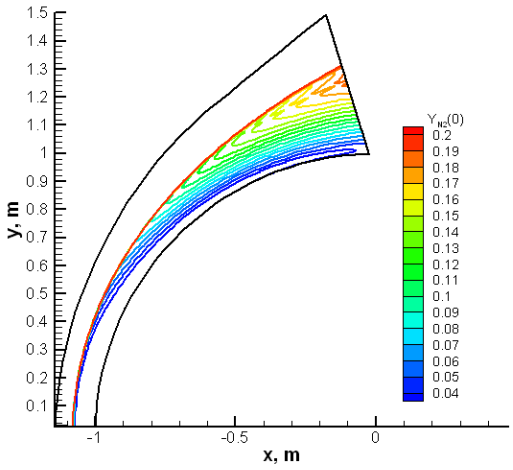

Figure 8. N_2(v=0) population density contours.
2260 processes (VT-m + VT-m-D + VV-m-D + VT-a) are included in the computations.
Effect of the VT excitation by atomic impact :
2125 processes VT-a are included in the computations in addition to the 135 other processes included before.

Figs. 8 and 9 show the contours of N_2(v=0) and N_2(v=3) population densities throughout the shock layer. It is interesting to notice how the various vibrational levels are populated in the shock layer. For example, in Fig. 7, the level v=0 depopulates immediately through the shock wave along the stagnation line, while this level

remains populated in the entire width of the shock layer in the flow acceleration region. This is explained by the fact that in the acceleration region the molecules are transported faster than they can interact with other particles to release part of their vibrational energy.

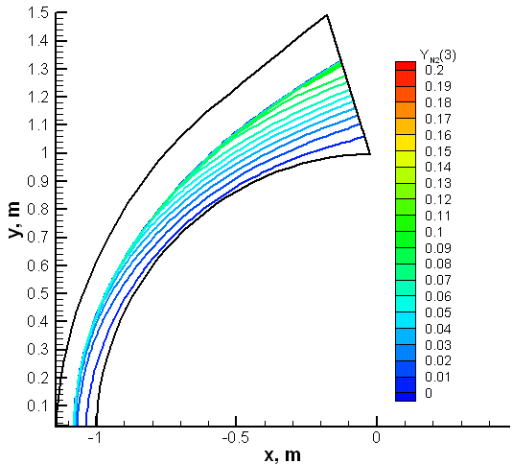

Figure 9. N_2(v=3) population density contours.
2260 processes (VT-m + VT-m-D + VV-m-D + VT-a) are included in the computations.
Effect of the VT excitation by atomic impact :
2125 processes VT-a are included in the computations in addition to the 135 other processes included before.

level. Interestingly, the temperature profile along the stagnation line slightly increases up to the boundary layer where the temperature drops to reach to wall temperature.

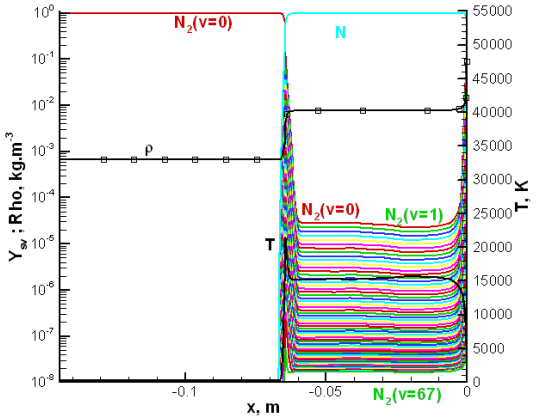

Figure 10. Temperature and mass fractions of N_2 (v=0,67) and N along the stagnation line.
2328 processes (VT-m + VT-m-D + VV-m-D + VT-a) are included in the computations.
Effect of the VT excitation by atomic impact leading to dissociation :
68 processes VT-a-D are included in the computations in addition to the 2260 other processes included before.

4.6 VT-m + VT-m-D + VV-m-D + VT-a + VT-a-D: 2328 Processes

Adding the 68 reactions corresponding to the vibration—translation exchanges by atomic impact leading to dissociation (VT-a-D) results in a complete dissociation of N_2 (v) (see Fig. 10). The flow field is strongly affected by the introduction of these additional reactions: again, the shock standoff distance is decreased (from 8.5 cm to 6.5 cm) and the temperature peak in the shock front is decreased from 43,000 K (Fig. 6) to 20,000 K (Fig. 10). Regarding the species densities, if the curves show that the various vibrational levels are all populated through the shock front, they are depopulated right behind the shock wave. This means that the additional reactions corresponding to the VT processes by atomic impact leading to dissociation (VT-a-D) are very efficient by transferring translational energy of atoms to vibrational energy of N_2 (v) in order to dissociate the molecules, whatever their vibrational

4.7 Is Boltzmann Distribution Reached in the Shock Layer ?

In order to show if the distribution of the vibrational level populations follows a Boltzmann distribution, Boltzmann plots of the N_2 vibrational levels at different positions behind the shock front (marked 01 to 12) are presented in Figs 11 and 12. The Boltzmann distribution is reached when the curves representing the level populations (or mass fractions) – expressed in a logarithmic scale – versus the energies of the levels – expressed in a linear scale – are linear. The Boltzmann diagrams plotted in Fig. 11, show that the Boltzmann distribution is not reached for the case (VT-m) + (VT-m-D) + (VV-m-D). On the other hand, the Boltzmann distribution is reached after a distance of 5 mm behind the shock front in the case (VT-m) (not shown), 8.5 mm behind the shock front for the case (VT-m) + (VT-m-D) + (VV-m-D) (not shown), and 15 mm behind the shock front for the case (VT-m) + (VT-m-D) + (VV-m-D) + (VT-a) + (VT-a-D) (Fig. 12).

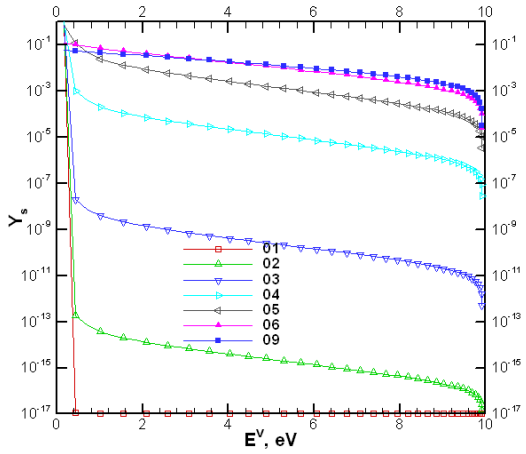

Figure 11. Boltzmann plots across the shock wave : Processes
(VT-m) + (VT-m-D) + (VV-m-D)
are included.

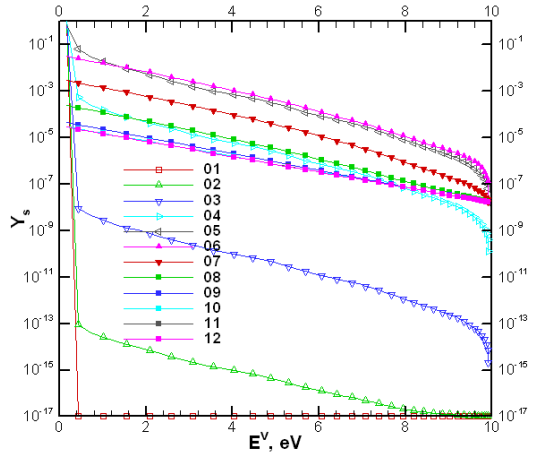

Figure 12. Boltzmann plots across the shock wave : Processes
(VT-m) + (VT-m-D) + (VV-m-D) + (VT-a) + (VT-a-D)
are included.

4.8 Comparison of Results Obtained with Detailed and Global Kinetics Rate Models

Comparisons between results obtained with detailed models and results obtained with global models (Park, Dunn-Kang, Gupta, CORIA) show how the global models perform compared to the detailed models in the prediction of the chemical species and vibrational states evolution past a shock wave (see Fig. 13 and a close-up view of the shock wave region in Fig. 14). Slight differences are observed in Fig.14 for the shock position predicted by the 4 global models, which are due to the differences in chemical kinetics rates provided by each global model. On the other hand, a very good agreement is observed between the results predicted with the detailed kinetics models and those predicted with the global model from CORIA.

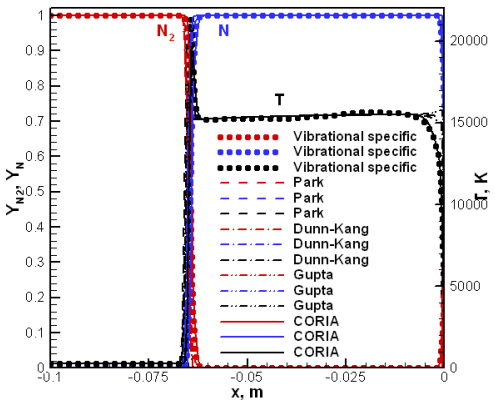

Figure 13. N and N_2 total mass fractions, and gas temperature along the stagnation line of the shock layer flow. Comparison between detailed (vibrational-specific, 2328 processes) and global (Park, Dunn-Kang, Gupta, CORIA) chemical kinetics models.

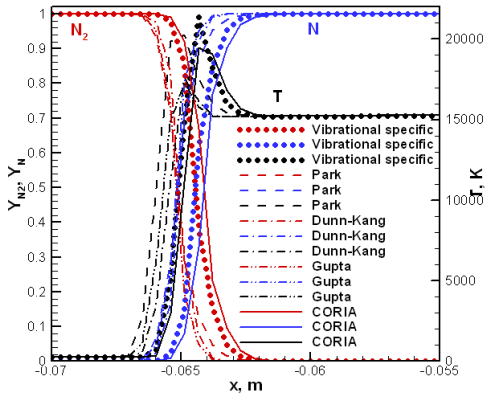

Figure 14. N and N_2 total mass fractions, and gas temperature along the stagnation line of the shock layer flow. Comparison between detailed (vibrational-specific, 2328 processes) and global (Park, Dunn-Kang, Gupta, CORIA) chemical kinetics models. Close-up view of Fig. 13.

5. CONCLUSION

This work shows the ability of Navier-Stokes codes to handle detailed kinetics models to compute the reactive and vibrational non-equilibrium gases in shock layers. The detailed model used in the present study has been implemented in the Navier-Stokes code PINENS step-by-step in order to show the effect of each group of chemical and vibrational processes in a given order. It was shown that the vibration—vibration exchanges do not have any visible effect on the present flow field, while the vibration—translation exchanges through molecular or atomic impact, leading to dissociation or not, are very efficient. Another main result is that the Boltzmann distribution of the vibrational levels is not reached until a certain distance behind the shock front. Finally, comparisons between results obtained with global and detailed chemical kinetics models show reasonably good agreement. Future work is oriented towards the implementation of detailed models for Earth and Mars atmospheres (respectively N_2-O_2 and CO_2-N_2) into the PINENS code in order to simulate the non-equilibrium and reactive gas throughout an axi-symmetric shock layer with detailed models and compare the results with those obtained with global models classically used in such simulations.

6. REFERENCES

1. Annaloro J., Bultel A., Omaly P. (2014). Collisional-radiative modeling behind shock waves in nitrogen, *Journal of Thermophysics and Heat Transfer*. 28(4).

2. Sanders R., Morano E., Druguet M.-C. (1998). Multidimensional Dissipation for Upwind Schemes: Stability and Applications to Gas Dynamics. *Journal of Computational Physics.* 145(2).

3. Druguet M.-C., Candler G.V., Nompelis I. (2005). Effect of Numerics on Navier-Stokes Computations of Steady Hypersonic Double-Cone Flows. *AIAA Journal.* 43(3).

4. Esposito F., Armenise I., Capitelli M. (2006). N-N_2 state-to-state vibrational-relaxation and dissociation rates based on quasiclaisscal calculations, *Chemical Physics.* 331(1).

5. Armenise I., Esposito F., Capitelli M. (2007), Dissociation-recombination models in hypersonic boundary layer flows, *Chemical Physics*. 336(1).

6. Landau L., Teller E.. (1936). Zur theory der Schalldispersion, *Physik. Z. Sowjetuion*. 10(34).

7. Millikan R.C., White D.R.. (1963), Systematics of vibrational relaxation, *Chemical Physics.* 39(12).